



Shifts in Greenland interannual climate variability lead Dansgaard-Oeschger abrupt warming by hundreds of years

5 Chloe A. Brashear¹, Tyler R. Jones¹, Valerie Morris¹, Bruce H. Vaughn¹, William H.G. Roberts², William B. Skorski¹, Abigail G. Hughes¹, Richard Nunn³, Sune Olander Rasmussen⁴, Kurt M. Cuffey⁵, Bo M. Vinther⁴, Todd Sowers⁶, Christo Buizert⁷, Vasileios Gkinis⁴, Christian Holme⁴, Mari F. Jensen⁸, Sofia E. Kjellman⁹, Petra M. Langebroek⁸, Florian Mekhaldi¹⁰, Kevin S. Rozmiarek¹, Jonathan W. Rheinländer⁸, Margit Simon⁸, Giulia Sinnl⁴, Silje Smith-Johnsen⁸, James W.C. White¹¹

10 ¹ Institute of Arctic and Alpine Research, University of Colorado, Boulder, CO, USA

² Geography and Environmental Sciences, Northumbria University, Newcastle-upon-Tyne, UK

³ National Science Foundation Ice Core Facility, Lakewood, CO, USA

⁴ Centre for Ice and Climate, Section for the Physics of Ice, Climate, and Earth, Niels Bohr Institute, University of Copenhagen, Copenhagen, Denmark

15 ⁵ Department of Geography, University of California, Berkeley, CA, USA

⁶ Department of Geosciences, Pennsylvania State University, University Park, Pennsylvania, USA

⁷ College of Earth, Ocean and Atmospheric Sciences, Oregon State University, Corvallis, Oregon, USA

⁸ Bjerknes Center for Climate Research, University of Bergen, Bergen, Norway

⁹ Department of Geosciences, UiT The Arctic University of Norway, Tromsø, Norway

20 ¹⁰ Department of Geology, Lund University, Lund, Sweden

¹¹ College of Arts and Sciences, University of North Carolina, Chapel Hill, NC, USA

Correspondence to: Chloe Brashear (chloe.brashear@colorado.edu)

25 **Abstract.** During the Last Glacial Period (LGP), Greenland experienced approximately thirty abrupt warming phases, known as Dansgaard-Oeschger (D-O) Events, followed by cooling back to baseline glacial conditions. Studies of mean climate change across warming transitions reveal indistinguishable phase-offsets between shifts in temperature, dust, sea salt, accumulation and moisture source, thus preventing a comprehensive understanding of the “anatomy” of D-O cycles (Capron et al., 2021). One aspect of abrupt change that has not been systematically assessed is how high-

30 frequency, interannual-scale climatic variability surrounding mean temperature changes across D-O transitions. Here, we utilize the EGRIP ice core high-resolution water isotope record, a proxy for temperature and atmospheric circulation, to quantify the amplitude of 7-15 year isotopic variability for D-O events 2-13, the Younger Dryas and the Bølling-Allerød. On average, cold stadial periods consistently exhibit greater variability than warm interstadial periods. Most notably, we often find that reductions in the amplitude of the 7-15 year band led abrupt D-O warmings

35 by hundreds of years. Such a large phase offset between two climate parameters in a Greenland ice core has never been documented for D-O cycles. However, similar centennial lead times have been found in proxies of Norwegian Sea ice cover relative to abrupt Greenland warming (Sadatzki et al., 2020). Using HadCM3, a fully coupled general circulation model, we assess the effects of sea ice on 7-15 year temperature variability at EGRIP. For a range of stadial and interstadial conditions, we find a strong relationship in line with our observations between colder simulated mean

40 temperature and enhanced temperature variability at the EGRIP location. We also find a robust correlation between year-to-year North Atlantic sea-ice fluctuations and the strength of interannual-scale temperature variability at EGRIP. Thus, both paleoclimate proxy evidence and model simulations suggest that sea ice plays a substantial role in high-frequency climate variability prior to D-O warming. This provides a clue about the anatomy of D-O Events and should be the target of future sea-ice model studies.



45 **1 Introduction**

1.1 Dansgaard-Oeschger Events

Stable isotopes of hydrogen (δD) and oxygen ($\delta^{18}O$) in polar ice cores provide information about local temperature and atmospheric circulation (Dansgaard, 1964). In Greenland, measurements of $\delta^{18}O$ and δD during the Last Glacial Period (LGP; 115-12 ka) reveal recurrent alternations, referred to as Dansgaard-Oeschger (D-O) cycles, between quasi-stable warm periods (i.e. Greenland Interstadials; GI) and cold baseline conditions (i.e. Greenland Stadials; GS) (Dansgaard et al., 1993). Global climate change associated with GI phases includes increased aridity across North America and Eurasia (Wagner et al., 2010; Asmerom et al., 2010), a northward shift of the tropical rain belt (Cruz et al., 2005; Deplazes et al., 2013), and antiphase warm periods in Antarctica (Blunier et al., 1998; Blunier & Brook, 2001; EPICA Community Members, 2006). It is widely accepted that these changes are linked via fluctuating strengths of the Atlantic Meridional Ocean Circulation (AMOC), in which GI and GS phases are characterized by strong and weak overturning, respectively (Broecker, 1998; Knutti et al., 2004, Stocker & Johnsen 2003). Abrupt GS-GI transitions have received widespread attention due to the unusual rate and magnitude of climatic change. For example, Greenland temperature increases of 5-16.5 °C occurred in a matter of decades (Huber et al., 2006b; Kindler et al., 2014; Severinghaus et al., 1998; Severinghaus & Brook, 1999). Despite decades of research, the trigger of this phenomenon and associated global changes is still debated.

1.2 Sea Ice

North Atlantic sea ice is often referenced in explanations of D-O warming because of its rapid response to relatively weak forcing and its influence on both atmospheric and oceanic dynamics. Several model simulations (Li et al., 2005; Li et al., 2010; Boers et al., 2018; Dokken et al., 2013; Petersen et al. 2013) show sea-ice displacements in the North Atlantic and Nordic Seas, complimented by associated feedbacks, can produce abrupt temperature increases consistent with those documented by water isotopes in Greenland ice cores. Though model reconstructions vary slightly, a primary mechanism for abrupt warming includes initial sea-ice reductions amplified by oceanic heat loss to the atmosphere, perturbations to the ocean salinity gradient, and decreased surface albedo.

Determining the driver(s) of tipping-point sea-ice displacements, in relation to abrupt Greenland warming, requires a highly resolved chronology of pertinent regional changes. Biomarker evidence from ocean sediment cores confirms that sea ice in the southern Norwegian Sea consistently experienced millennial-scale oscillations in pace with D-O cycles (Hoff et al., 2016). In one core location, ice cover reductions began during the late GS phase, thus leading abrupt warming by hundreds of years (Sadatzki et al., 2019, Sadatzki et al., 2020). However, these ocean sediment cores have low-resolution (i.e. multi-decadal scale sampling) and their age chronologies have large uncertainties. By comparison, Greenland ice cores can reach annual or multi-year resolution. For this reason, they have been key in establishing leads and lags of various geological parameters, deducing causal relationships, and disentangling the spatiotemporal progression of abrupt climate change. Observations of dust, moisture source and accumulation during D-O warming exhibit indistinguishable (Capron et al., 2021) or near synchronous (Steffensen et al., 2008) shifts, suggesting



widespread regional climate changes in the North Atlantic and Greenland occurred in phase. This is partly at odds with evidence from Norwegian Sea sediment cores.

1.3 Climate Variability

85 To further investigate leads and lags during abrupt D-O warmings, we utilize the EGRIP water isotope (δD) record to assess the temporal evolution of mean temperature vs. high-frequency water isotope variability in Northeastern Greenland. Variability in Greenland ice cores has long been studied, but coarse analytical sampling on increasingly compressed annual ice layers has limited LGP analyses to centennial- or millennial-scales (WAIS Divide Project Members, 2015; Rehfeld et al., 2018; Schulz et al., 2004). Similarly, interpretations of interannual- and decadal-scale
90 Greenland climate variability have primarily been available for the Holocene (Hughes et al., 2020; Rimbu & Lohmann, 2010; Rimbu et al., 2021; Ortega et al., 2014). Though studies assessing decadal-scale variability during the LGP exist (Boers et al., 2018; Ditlevsen et al., 2002), the data sets used were discretely sampled at cm-scale resolutions which may diminish or conceal important high-frequency climatic information (Fig. A1). Developments in continuous-flow sampling techniques have recently allowed for high-frequency analysis of water isotope variability in Antarctic ice
95 cores during the LGP by preserving the amplitude of interannual-scale signals (Jones et al., 2017a; Jones et al., 2018). In the case of West Antarctica, a shift in LGP interannual isotopic variability was linked to broad changes in Pacific Basin teleconnection strength driven by reductions in Laurentide Ice Sheet topography and changing albedo (Jones et al., 2018). This study demonstrated that the drivers of high-frequency climate variability can temporally decouple from the drivers of mean local climate (e.g. temperature, accumulation, etc.), providing new insights about paleoclimate
100 dynamics.

In the northern high latitudes, sea ice varies substantially on multi-year and multi-decade bases, imparting variability into the climate system on similar timescales. The Greenland water isotope variability record may therefore provide clues about high-frequency sea-ice variations as such shifts would affect the isotopic signature of precipitation via
105 influences on both moisture source and atmospheric circulation. Our study comprises of four parts: 1) comparison of LGP isotopic variability relative to the Holocene, 2) comparison of isotopic variability between warm Greenland Interstadials (GI) and cold Greenland Stadials (GS), 3) a moving window assessment of lead-lag relationships between isotopic variability and mean temperature increases associated with D-O Events and 4) a model assessment of LGP North Atlantic temperature and sea-ice variability at interannual scales using the general circulation model HadCM3,
110 including how simulated sea-ice variability affects temperature variability at the EGRIP site.

2 Methods

2.1 Water Isotope Data

The EGRIP (East Greenland Ice Core Project) ice core was drilled at 75°38' N and 35°60' W from an interior
115 location of the North East Greenland Ice Stream (NEGIS). δD and $\delta^{18}O$ records were measured using a semi-automated continuous flow analysis (CFA) system in conjunction with a Picarro cavity ring down laser spectrometer (CRDS; model L2130-i) (Jones et al., 2017a). The CFA-CRDS system is constituted by three subsystems: the ice



120 core melter, a liquid-to-vapor phase conversion, and the isotopic analyzer. Ice core sticks measuring $100 \times 1.3 \times 1.3$ cm are melted at a rate of 2.5 cm/min by an aluminum plate maintained at 14.6°C. Melt water is pulled through the preparation line via peristaltic pumps where it is filtered to remove particulates, degassed, and aerosolized by a nebulizer. Finally, ice core derived water vapor is introduced to the CRDS in a continuous, stable stream for optimal performance. Precise δD and $\delta^{18}O$ measurements are derived in real time relative to Vienna Standard Mean Ocean Water (VSMOW; $\delta^{18}O = \delta D = 0$ per mil). Using this CFA methodology, the water isotope record has a sample resolution of ~ 1 mm throughout, with an effective resolution of ~ 5 mm due to mixing. Figure A1 demonstrates the artificial loss of interannual amplitudes with depth for coarser (i.e. cm-scale) sampling resolutions.

130 To date, the EGRIP water isotope record extends to ~ 49.9 ka b2k (thousands of years before 2000 CE) according to the Greenland Ice Core Chronology (GICC05) (Svensson et al., 2008) (Fig. 1a). The GICC05 was transferred to EGRIP using 373 tie points between 0-14.96 ka b2k (Mojtabavi et al., 2019) and an additional 138 tie points between 14.96-49.9 ka b2k (Gerber et al., 2021). For each EGRIP data point (in mm-resolution), the corresponding NGRIP depth was obtained by linear interpolation between tie points and age was determined from the annual-layer counted GICC05 timescale. The ages used here inherit the maximum counting error of the GICC05 timescale. In addition, the interpolation introduces an uncertainty which is relevant when comparing to other records on the GICC05 timescale. Isotope data is interpolated at a uniform time interval of 0.05 years. On average, temporal differences in adjacent data points range from sub-weekly in the Holocene to sub-monthly during the LGP.

2.2 Spectral Analysis

140 We use a multi-taper method (MTM) of spectral analysis (Huybers, 2021; Percival & Walden, 1993) to calculate spectral power densities which are later converted to relative amplitudes within the 7-15 year band. MTM spectral analysis averages multiple realizations of data using a series of Slepian tapers, offering a smoothed estimate of prominent spectral characteristics. We spectrally analyze the EGRIP δD record in 400-year windows with a timestep of 50 to 200 years, depending on desired temporal resolution. A window size of 400 years provides adequate repetition of interannual to decadal signals for precise estimation of high-frequency power density spectra.

145 2.3 High-Frequency Signal Attenuation

Firn is a porous and permeable substance comprised of snow and ice at the surface of an ice sheet. Water vapor within interconnected firn pathways diffuses along temperature and concentration gradients. Isotopic exchange occurs at four interfaces (e.g. (1) vapor-vapor, (2) vapor-ice surface, (3) ice surface-ice interior and (4) through the ice matrix), altering the isotopic composition of deposited precipitation (Whillans & Grootes, 1985). Vapor phase diffusion disproportionately dampens high-frequency signals but ceases below a pore density of 804 kg m^{-3} (Johnsen et al., 2000). Solid phase diffusion continues below the pore close off depth at a considerably slower rate (Jones et al., 2017). Spectral analysis is used to interpret the extent of vapor and solid phase diffusion to single frequency bands (Fig. A2). At EGRIP, the annual signal (i.e. 1 year) cannot be resolved, while the 2-5 year signals are significantly dampened



155 throughout the LGP and Holocene. The 7-15 year band is well persevered throughout the entire EGRIP record, and is thus the focus of this analysis.

2.4 Gaussian Diffusion Correction

160 Values of cumulative mean water molecule diffusion, known as “diffusion lengths”, can be estimated for windows of time or depth along a water isotope signal by evaluating dampened sections of its high-frequency spectrum (Gkinis et al., 2014; Hughes et al., 2020; Johnsen et al., 2000; Jones et al., 2017b; Jones et al. 2018; Jones et al. 2023; Kahle et al., 2021; Simonsen et al., 2011). Diffusion lengths are equivalent to the estimated standard deviation (i.e. sigma) of water molecule diffusion, which describes the statistical vertical displacement of water molecules from their original position (Fig. A3; Johnsen et al., 2000). The power density spectrum of a diffused water isotope signal, $P(f)$, is defined as

165

$$P(f) = P_o(f) \exp [-(2\pi f \sigma_a)^2] \quad (1)$$

where $P_o(f)$ is the power density spectrum of the undiffused signal (in units of per $\text{mil}^2 \text{ yr}$), f is frequency (in units of $1/\text{yr}$), and σ_a is diffusion length (in units of years). To solve for σ_a , we create twelve equally spaced logarithmic bins within the diffused interval and fit a Gaussian to $P(f)$ using a least-squares fitting technique) (Fig. A4). Diffusion lengths can be expressed in meters (σ_z) using the conversion:

170

$$\sigma_z = \sigma_a * \lambda_{\text{avg}} \quad (2)$$

where λ_{avg} is mean annual layer thickness (in units of m/yr). The diffusion corrected power density spectra, $P_o(f)$, is determined by rearranging equation (1), so that:

$$P_o(f) = P \exp [4\pi^2 f^2 \sigma_a^2] \quad (3)$$

175 where P is the observed power density, f is frequency, and σ_a is the solved diffusion length. We calculate average undiffused power density, P_{ave} , in the 7-15 year band by dividing the integral of power density by the frequency range (Jones et al. 2018):

$$P_{\text{ave}} = \frac{\int_{f_a}^{f_b} P_o(f)}{f_b - f_a} \quad (4)$$

180 where f_a and f_b are the upper and lower limits of the frequency band, respectively. Relative strength (P_{amp}), or amplitude, is calculated for each window as the square root of average power density (P_{ave}):



$$P_{amp} = \sqrt{P_{ave}} \quad (5)$$

2.5 Uncertainty

Diffusion length, σ_a , can also be quantified as the slope, m , of a linear regression, y , fitted to $\ln[P(f)]$ versus f^2 of the
185 diffused interval. Uncertainty bounds are defined as maximum and minimum slopes within one standard deviation of
 y (Jones et al. 2017b, 2018) (Fig. A4).

2.6 HadCM3

To investigate the physical processes underlying our results, we utilize the fully-coupled HadCM3 ocean-atmosphere
190 general circulation model (GCM) to test how global climate responds to various forcing mechanisms in the North
Atlantic (Gordon et al., 2000; Pope et al., 2000; Valdes et al., 2017). The simulations used here (Roberts and Hopcroft,
2020) force LGP stadial phases through the imposition of a freshwater flux or a perturbation to annual mean sea-ice
cover. The hosing simulations impose freshwater uniformly across the North Atlantic between 50° to 70° N and include
variations in flux between 0.04 and 1.0 Sv ($10^6 \text{ m}^3 \text{ s}^{-1}$). The perturbed sea-ice simulations artificially pin ice extent
195 to a particular latitude between 40° to 70° N, though interannual ice edge variability is still possible due to advection
in the module. Ice depth is prescribed to 4 meters and may reach a maximum concentration of 95%. To deconvolve
how climate responds to both sea-ice and freshwater hosing, a forcing which combines the aforementioned simulations
is included. To investigate a possible dependence on background climate state, we also impose the sea-ice and
freshwater forcing onto boundary conditions simulating both the Last Glacial Maximum (LGM) and Pre-Industrial
200 (PI). We calculate high-frequency, interannual-scale variability as the standard deviation of 7-15 year band pass filtered
timeseries for temperature and sea-ice concentration output.

The freshwater hosing and pinned sea-ice simulations give a range of mean temperatures at the location of EGRIP that
represent a spectrum of possible mean LGP climate states. With this spectrum of change, we reduce the bias that could
205 arise from defining a single stadial or interstadial state with only one forcing mechanism. Both forcings alter the
distribution of sea ice, however the freshwater forcing also imposes a large, and potentially unrealistic, change to ocean
circulation. Crucially, including these two sets of simulations controls for oceanic-driven effects when investigating
the role of sea ice in driving climatic variability at EGRIP: if a response is general across all simulations, even for
pinned sea-ice simulations with no change in ocean circulation, we can infer that ocean circulation is not the immediate
210 cause of the change.

3 Results

3.1 Interannual Water Isotope Variability

The raw EGRIP δD record exhibits millennial-scale D-O variability consistent with prior analyses of deep ice cores
215 (e.g. GRIP, NGRIP) recovered from inland Greenland (Fig. 1a) (Greenland Ice-core Project (GRIP) Members,



1993; North Greenland Ice Core Project Members, 2004). Isotopic measurements range from approximately -240 to -310 per mil in the Holocene while the LGP is characterized by increased depletions and greater spread in values ranging from -260 to -380 per mil. On average, diffusion-corrected variability in the 7-15 year band is elevated during the LGP, compared to the Holocene, reaching a maximum plateau between ~30-15 ka b2k. The average decrease in variability between the plateau and the Holocene is approximately 60% (Fig. 1b). Large variations in 7-15 year variability during the LGP are evident. For example, the 7-15 year amplitude at ~38 ka b2k is so low that it is nearly the same magnitude as variability seen throughout the Holocene. Conversely, variability at ~29.5 ka b2k is ~360% greater than in the Holocene.

225 Within the context of the LGP, high-frequency variability is on average 18% lower in the 400 years following the onset of warm GI periods, relative to the onset of preceding cold GS periods (Rasmussen et al., 2014) (Fig. 2b). The largest reduction in variability from GS-onset to GI-onset is 37% for D-O Event 8, while the smallest change is indistinguishable from zero for D-O Event 9. In the case of D-O Event 9, the temporal length of the interstadial is only 260 years, which skews 400-year averages towards the background stadial state. There are no instances of greater variability during an GI-onset, relative to the prior GS-onset (Table 1). The above analyses demonstrate a negative correlation between water isotope ratios (δD) (which are a proxy for temperature) and strength (i.e. amplitude) of interannual and decadal isotopic variability in Northeastern Greenland throughout the last 50 kyr (Fig. 1c, 1d). It is important to note that we document multi-millennial excursions in variability occurring between 27-15 ka b2k wherein cold GS conditions persist uninterrupted by abrupt warming, with the exception of D-O Events 5.1 and 5.2 around 23 ka b2k which do not appear to be associated with a detectable change in 7-15 year variability. The excursions are comparable, yet generally smaller in magnitude than those occurring between 50-27 ka b2k when D-O cycling is relatively consistent.

	D-O Event												
	2	3*	4*	5.1*	5.2	6*	7	8	9*	10	11	12	13
GS	133.2	132.4	157.2	126.5	141.8	106.5	124.6	106.5	94.5	117.5	118.1	113.4	101.6
GI	124.5	125.4	99.2	123.5	86.6	98.8	94.3	59.8	117.5	95.6	96.8	76.5	72.9
%	6.0	20.2	21.5	12.9	18.6	20.6	11.4	36.7	-0.05	18.9	14.6	24.6	-

240 **Table 1** | Percent (%) reduction in 7-15 year diffusion-corrected variability (per mil² yr) between Greenland Stadial (GS) onset and the following Greenland Interstadial (GI); D-O Events marked by an asterisk are characterized by interstadial phases shorter than the 400 year window size (240, 300, 240, 380, 260 years for D-O Events 3, 4, 5.1, 6, and 9, respectively) (Rasmussen et al., 2014)

245 Next, we reduce the timestep of our 400-year window analysis from 200 to 50 years to analyze the lead-lag relationship between mean temperature change associated with D-O Events and isotopic variability (Fig. 3a, 3b). In most instances (i.e. D-O Events 2.2, 3, 4, 5.1, 5.2, 6, 7, 8, 9, 10, 12 13), we find that the reduction in 7-15 year variability from peak



values initiates ~150-600 years **prior** to abrupt warming (Fig. 4). There is only one case (i.e. D-O Event 11) in which the reduction in isotopic variability leads warming on sub-centennial scales. Due to our window size of 400 years, we
250 can only conclusively say that lead times of > 200 years are significant beyond uncertainty of the diffusion correction. Thus, there is clear evidence that 7-15 year variability for D-O Events 2.2, 3, 4, 5.2, 6, 7, 8, 10, 12 and 13 leads mean temperature change at the onset of GI phases.

3.2 HadCM3 Model Output

255 Interannual-scale (i.e. 7-15 year) temperature variability is assessed for Northeastern Greenland and the broader North Atlantic region. We find that temperature variability and mean temperature at the EGRIP site are negatively correlated (i.e. colder states are characterized by greater fluctuations in atmospheric temperature and vice versa) (Fig. 6b). These results agree well with our observations. To understand a wider regional context of temperature variability, we show a correlation map of 7-15 year variability across the North Atlantic relative to the 7-15 year variability at the EGRIP
260 field site (Fig. 5a). Figure 5a shows the strongest remote correlation outside of Greenland exists in the North Atlantic subpolar gyre region, southwest of Iceland, and extending into the southernmost portion of the Norwegian Seas. Oceanic regions north of Iceland and east of Greenland (i.e. central Nordics Seas) show very low correlation (Fig. A6).

Next, we investigate the role of year-to-year sea-ice fluctuations on climate variability over Northeastern Greenland.
265 Figure 5b displays the spatial correlation between 7-15 year sea-ice and temperature variability over Northeastern Greenland. Again, model output suggests ties between EGRIP and the North Atlantic, with the strongest correlations near 50° N 30° W. Figure 6a shows the individual simulation results at 50° N 30° W, with all simulations showing a trend of increased EGRIP temperature variability with increased sea-ice variability. In the Nordic Seas, simulations exhibit little to no correlation between interannual-scale sea-ice fluctuations and temperature variability at EGRIP (Fig.
270 A7). This finding is consistent with a persistent ice cover throughout both stadial and interstadial conditions (Li et al., 2010; Hoff et al., 2016; Sadatzki et al. 2020), wherein ice variability is inherently low.

Correlation does not demonstrate causation, so we examine other factors which might explain our results. Changes in sea-ice variability might be associated with changes in mean temperature or with total sea-ice area. Therefore, we
275 compare the strength of these variables in explaining trends of high-frequency temperature variability at the EGRIP location. Figure 6b shows how EGRIP temperature variability covaries with mean temperature. There is a strong negative correlation for all simulations, except those marked by grey crosses (Fig. 6b). This subset of simulations contains unrealistic sea-ice prescriptions (i.e. sea ice extends south of 50° N) (Brennan et al., 2013; Dokken et al., 2013; Sadatzki et al. 2020). The extended sea-ice cover causes a reduction in temperature variability that is greater
280 than the reduced mean temperature would suggest; the grey crosses sit well below the regression line. Similarly, Figure 6c shows how EGRIP temperature variance covaries with total North Atlantic sea-ice area. We might expect that lower mean temperatures in Greenland are associated with extended sea-ice cover and it is therefore the mean sea-ice cover that affects EGRIP temperature variability. As with mean temperature, we find that the unrealistic sea-ice extent



simulations fall far from the regression line. Furthermore, the correlation amongst realistic simulations is low ($R^2 =$
285 0.45), relative to other comparisons. Thus, mean temperature and sea-ice extent alone cannot explain shifts in
temperature variability across LGP climate states. By contrast, a comparison between 7-15 year EGRIP temperature
variability and North Atlantic sea-ice variability exhibits higher agreement ($R^2 = 0.60$) for all simulations (i.e. both
realistic and unrealistic prescriptions); grey crosses fall on or near the regression line (Fig. 6a). This indicates a robust
relationship and crucially, that 7-15 year sea-ice fluctuations in the North Atlantic are an excellent predictor of EGRIP
290 temperature variability on similar scales.

4 Discussion

The results of this study are twofold. First, using HadCM3 we identify a critical coupling between interannual-scale
North Atlantic sea-ice fluctuations and high-frequency temperature variability over Northeastern Greenland throughout
295 the LGP. Conceptually, these results can be accounted for by our isotopic observations (i.e. stronger high-frequency
variability during GS periods, and vice versa). Glacial stadial phases are characterized by lower average temperature
and sea ice extending to the North Atlantic. It is possible that greater excursions in sea-ice concentration were driven
by the enhanced latitudinal range between maximum summer and winter ice extents (Sadatzki et al. 2020), which
presumably changed on a year-to-year basis. These seasonal variations would impart volatility in high-frequency
300 temperature fluctuations on annual, interannual, and decadal scales via ice-atmosphere feedbacks. By extension,
Rayleigh distillation and the isotopic signature of precipitation at EGRIP would also be impacted.

An additional contribution to enhanced isotopic variability during stadial phases may stem from altered source-to-sink
pathways. With large seasonal swings in the capping and exposure of the ocean surface by sea ice, evaporative sources
305 upstream of EGRIP would also be altered. As a consequence, variability in both evaporative source signatures and
temperature gradients of moisture transport to Northeastern Greenland would increase. An isotope enabled GCM is
required to test this hypothesis.

Our second, and key, finding is that reductions in 7-15 year isotopic variability generally begin hundreds of years prior
310 to abrupt D-O warming at the EGRIP site. Taken together with results from HadCM3, we suggest that a fundamental
change in North Atlantic sea-ice dynamics occurs in the centuries leading to Greenland warming. One possibility is
that winter maximum ice extent retracted north of the high correlation North Atlantic pocket (50° N 30° W) in the
centuries leading to abrupt D-O warming, thereby reducing the latitudinal range between seasonal extents and overall
mean ice extent. Based on our results from HadCM3, such a change would also be correlated with lower 7-15 year
315 temperature variability at EGRIP. Alongside this, greater exposed ocean surface in winter may increase winter
temperatures, ultimately increasing mean annual temperatures at EGRIP. Some GS phases (i.e. prior to D-O Events
5.2, 8, and 10) exhibit a small rise in δD in the centuries prior to abrupt temperature increase. It is possible the GS
phases which do not exhibit this behavior experience a muting of the δD increase due to source moisture deriving from
more northerly, isotopically-depleted water as the ice edge recedes.



320

The following section outlines a framework in which this hypothesis fits within the existing literature. It has been previously suggested that a salt oscillator in the North Atlantic drove bimodal shifts in AMOC and hence, transitions between stadial and interstadial conditions during the LGP (Broecker et al., 1990; Peltier & Vettoretti, 2014). Using HadCM3, Armstrong et al. (2022) demonstrates a complex ocean-atmosphere-ice feedback capable of maintaining a millennial-scale salt oscillation mechanism. To summarize, the salinity gradient between the tropics and North Atlantic regulates advection between these regions, thus governing the strength of AMOC, northward heat transport and related regional climate effects. In the model, the onset of cold stadial periods are marked by a sluggish AMOC, accumulating salinity in the tropics and diminishing salinity in the North Atlantic. Due to a reduction in the transport of dense (i.e. salty) and warm water north, deep-water formation drops to a minimum. Concurrently, the difference in PSU (i.e. Practical Salinity Unit) between the tropics and North Atlantic approaches a maximum. It is precisely this feature, peak salinity gradient, that kickstarts AMOC and initiates a transition from stadial to interstadial in the salt oscillator framework.

325

330

335

340

Sea ice and surface freshwater fluxes are deemed critical in developing the salinity gradient, though their effects are spatially heterogeneous. In the North Atlantic, both stadial and interstadial periods are characterized by a freshening effect. Winter ice traps freshwater by freezing sea water and trapping overhead precipitation. The summer melt season flushes out both freshwater sources, resulting in a net freshening effect. Due to reduced ice extent during interstadials, this freshening effect is dampened. A relevant detail of the salt oscillation mechanism is that North Atlantic salinity and AMOC strength begin to steadily increase partway through the stadial phase (i.e. centuries prior to interstadial onset), priming the system for an abrupt shift. Critically, Armstrong et al. (2022) proposes reduced regional freshening due to gradual sea-ice retreat as a likely cause. Our study provides paleoclimate and modeling evidence in favor of this suggestion.

345

350

355

A useful tool in corroborating the centennial-scale phase offset is empirical evidence of North Atlantic sea ice behavior with similar lead-lag behavior. Unfortunately, high-resolution records are sparse. One such analysis (Sadatzki et al., 2020) finds declining seasonal sea ice in the lower latitude Norwegian Sea (MD99-2284; 62° N, 0° W) initiated ice-free conditions further north (MD95-2010; 66° N, 04° E) prior to Greenland temperature increase. At the northern core site, a change in the properties of biomarkers Brassicasterol and HBI-III, occurring in open-ocean environments, is detectable centuries prior to the abrupt GS-GI transition. A direct comparison to our isotope variability timeseries shows near simultaneous shifts, possibly indicating a common link (Fig. 7). However, the MD95-2010 sediment core site falls just outside the high-correlation pocket suggested by HadCM3. One explanation is that large scale changes in Norwegian Sea mean ice extent are not associated with shifts in variability, unlike the North Atlantic. It is also possible the model grid cells are too coarse to resolve fine detail in Norwegian Sea ice movement, thus failing to detect shifts in variability as mean sea-ice area changes. Nevertheless, this realization prompts interest in high-resolution sea-ice proxy records at the heart of the high variance correlation.



360 Lastly, an inexplicable component of this study is the continuation of large excursions in high-frequency isotopic variability even when D-O cycling is turned off for long stretches (i.e. 27-15 ka b2k). In some cases, the fluctuations are comparable in magnitude to those occurring across prior GS-GI transitions. It seems a climate variability oscillation is inherent to the LGP background state, yet does not result in abrupt mean climate change (i.e. D-O Events) based on certain boundary conditions which remain to be seen. Due to the simultaneous occurrence of the Last Glacial Maximum during this timeframe, an obvious factor to test in future studies is the height and extent of the Laurentide and Scandinavian Ice Sheets and their effects on climate variability.

365 **5 Conclusion**

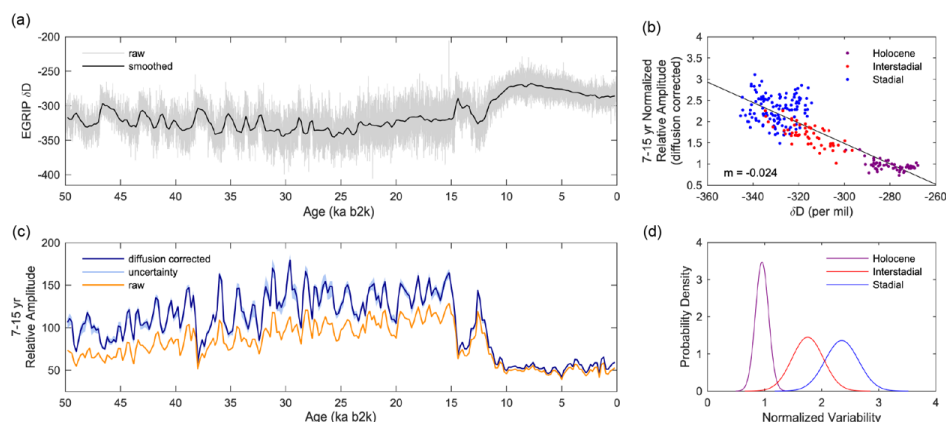
370 Interannual and decadal variability is an important aspect of paleo-climate reconstructions and assessments of D-O warming, but such records have been previously sampled at lower resolution, which may exclude important climate insights that are documented here. In this study, the mm-scale EGRIP water isotope record is used to quantify diffusion-corrected 7-15 year isotopic variability for Northeastern Greenland to 49.9 ka b2k. Importantly, we provide evidence that high-frequency LGP Greenland climate variability became decoupled from local mean temperature in the centuries preceding D-O warming. Our initial model analysis suggests lower latitude feedbacks associated with interannual North Atlantic sea-ice change may be a driver of this offset. As the cause of D-O cycles continues to be debated, these results should be considered.

375 Additionally, future isotope-enabled GCM studies may benefit from utilizing the high-frequency EGRIP variability timeseries, presented here, to constrain boundary conditions or benchmark model output. We suggest targeted tests aimed at temporally reconciling the centennial-scale offset with sea-ice behavior to better understand regional North Atlantic climate change within the context of abrupt D-O warming. Analysis of high-resolution sediment proxy records from critical locations identified in this study may also clarify uncertainties.

380

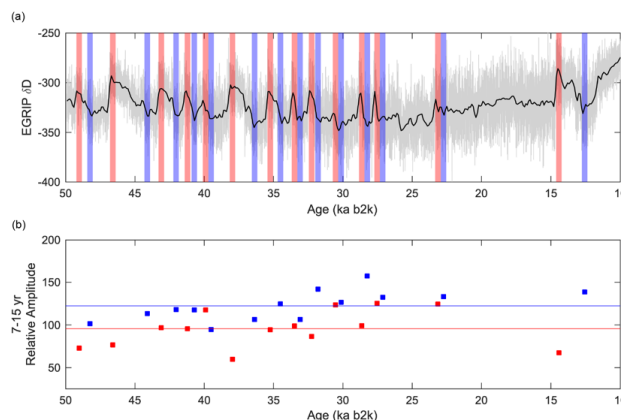


385



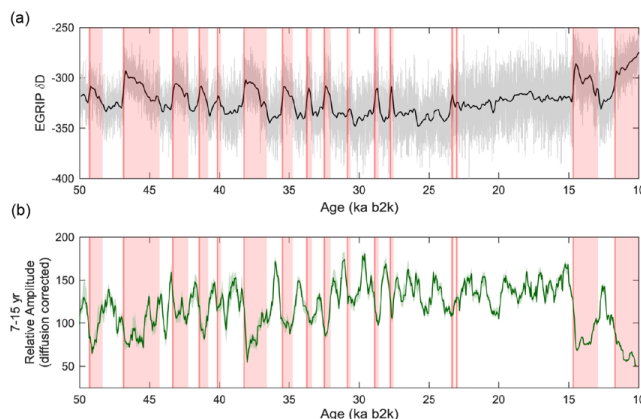
390 **Figure 1** | (a) EGRIP δD to 50 ka b2k (grey) overlaid by down-sampled data for visual clarity (black; window = 400 years; timestep = 200 years); (b) diffusion-corrected data from panel (c) binned by climate state and fit with linear regression ($r^2 = 0.75$; $p < 0.05$); (c) Raw (orange) and diffusion-corrected (blue) strength of 7-15 years isotopic variability at EGRIP (window = 400 years; timestep = 200 years); (d) variance in binned data from panel (b)

395

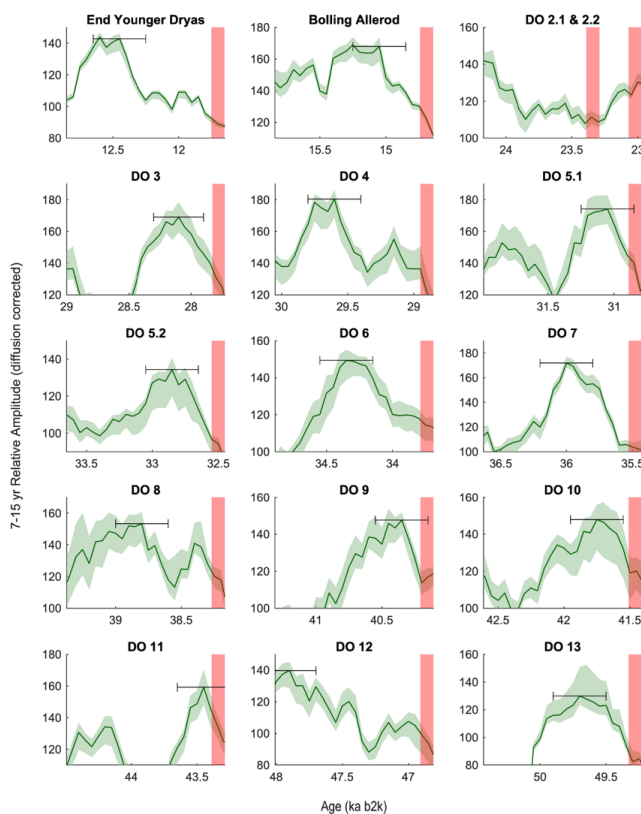


400 **Figure 2** | (a) EGRIP δD overlaid by 400-years windows at onset of Greenland Interstadial (GI; red) and Greenland Stadial (GS; blue) periods (Rasmussen et al., 2014); For GI phases of less than 400 years, the onset of the subsequent GS phase is defined as the termination of the GI window to avoid overlap; Due to the brief duration of D-O Events 2.1 and 2.2, one 400-year window is placed at the onset of D-O 2.2 (i.e. 23.34 ka b2k), which encompasses the entirety of D-O 2.1, a majority of D-O 2.2, and the short-lived stadial phase between each interstadial (b) diffusion-corrected 7-15 year variability of windows outlined in panel (a)

405

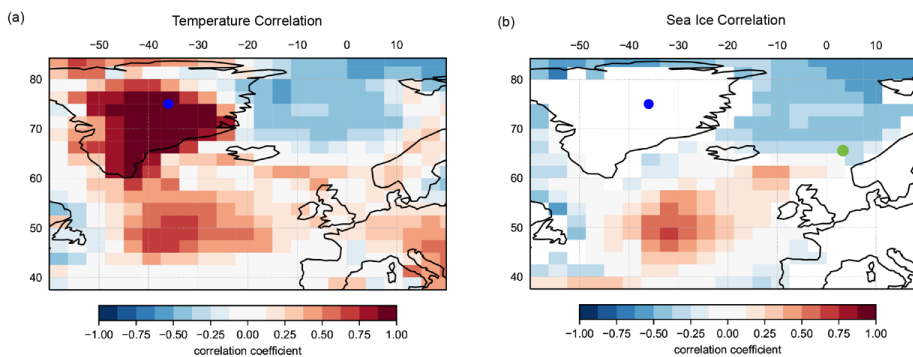


410 **Figure 3** | (a) EGRIP δD (black; window = 400 years; timestep = 50 years) shaded by duration of warm Greenland Interstadial periods 2-13, the Bølling-Allerød, and Holocene (red; Rasmussen et al., 2014); (b) high-resolution analysis of 7-15 year isotopic variability (dark green; window = 400 years; timestep = 50 years) with uncertainty bounds (light green)

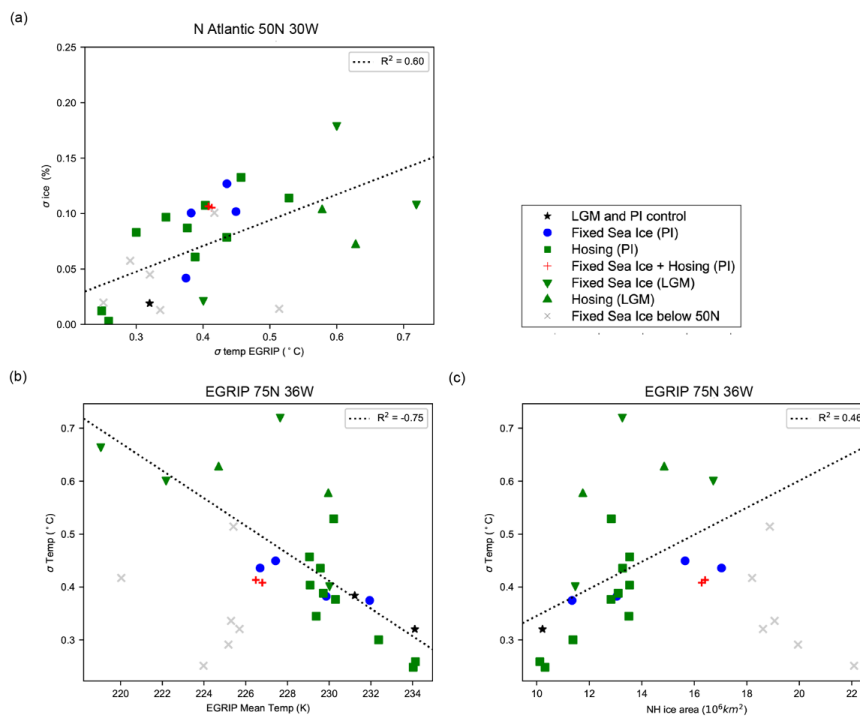


415 **Figure 4** | Zoomed view of GS-GI transitions from Figure 2 panel (d) for D-O Events 2-13, the Bølling-Allerød, and Holocene onset; high-resolution analysis of 7-15 year isotopic variability (dark green; window = 400 years; timestep = 50 years) with uncertainty bounds (light green); black horizontal error bar indicates 400-year window range at height of variability; red shading represents 50-year buffer before and after onset of GS-GI transition as defined in Rasmussen (2014)

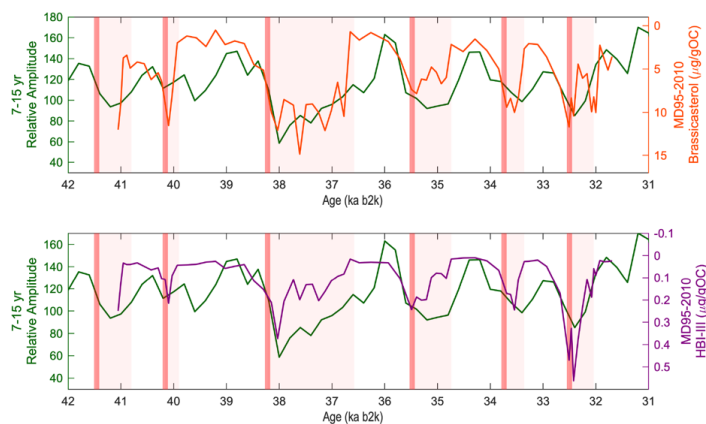
420



425 **Figure 5** | (a) Correlation between 7-15 year temperature variability at EGRIP (blue dot) and other regional grid cells; (b) Correlation between 7-15 year temperature variability at EGRIP (blue dot) and 7-15 year sea ice variability for all regional oceanic grid cells; red and blue shading depicts high and low correlations, respectively; MD95-2010 core site is marked by a green circle



430 **Figure 6** | Individual model results for (a) 7-15 year sea ice variability versus 7-15 year EGRIP temperature variability near the high-correlation North Atlantic pocket (i.e. 50°N 30°W) (b) 7-15 year temperature variability versus mean temperature at the EGRIP location (c) 7-15 year temperature variability versus Northern Hemisphere ice area at the EGRIP location; Note: simulations including sea ice extending below 50° N (grey x) have been excluded from regression
435

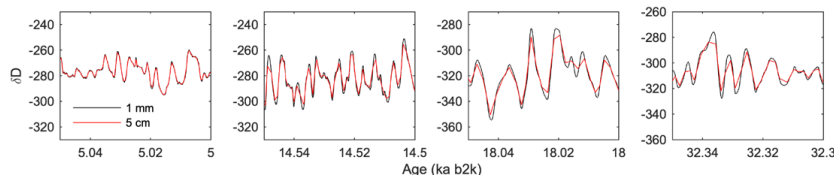


440 **Figure 7** | Comparison between 7-15 year diffusion correct isotopic variability at EGRIP and open ocean biomarkers
(i.e. HBI-III and brassicasterol) recovered from ocean sediment at 66° N, 04° E; dark red shading represents 50-year
445 buffer before and after onset of GS-GI transition; light red shading represents duration of GI period as defined in
Rasmussen (2014)

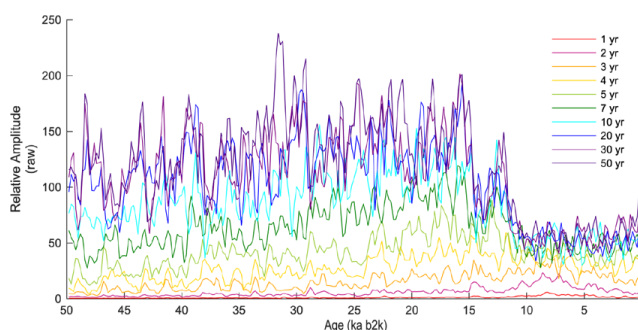
445



Appendix A: Figures

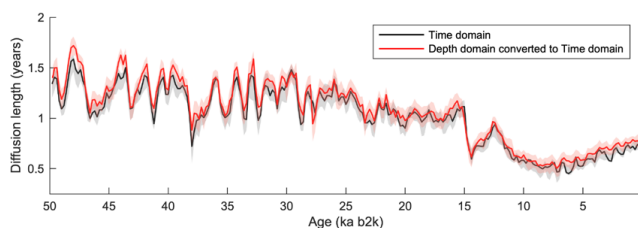


450 **Figure A1** | Comparison of original 1 mm-EGRIP δD (black) to downsampled 5-cm EGRIP δD (red); Each window contains 50 years of data with progressively older windows towards the right; lower sampling resolution artificially reduces the amplitude of interannual and decadal fluctuations after approximately 12 ka b2k



455 **Figure A2** | Strength of raw (i.e. non-diffusion corrected) isolated frequencies in the EGRIP δD record; Substantial attenuation with age due to diffusion in the firn layer is evident in the 1-5 year signals

460



465 **Figure A3** | Comparison of diffusion lengths calculated using the EGRIP δD record in the time domain (black) versus the depth domain converted to the time domain using annual layer thickness (red); uncertainties largely overlap with some deviations prior to 43 ka b2k.

470



475

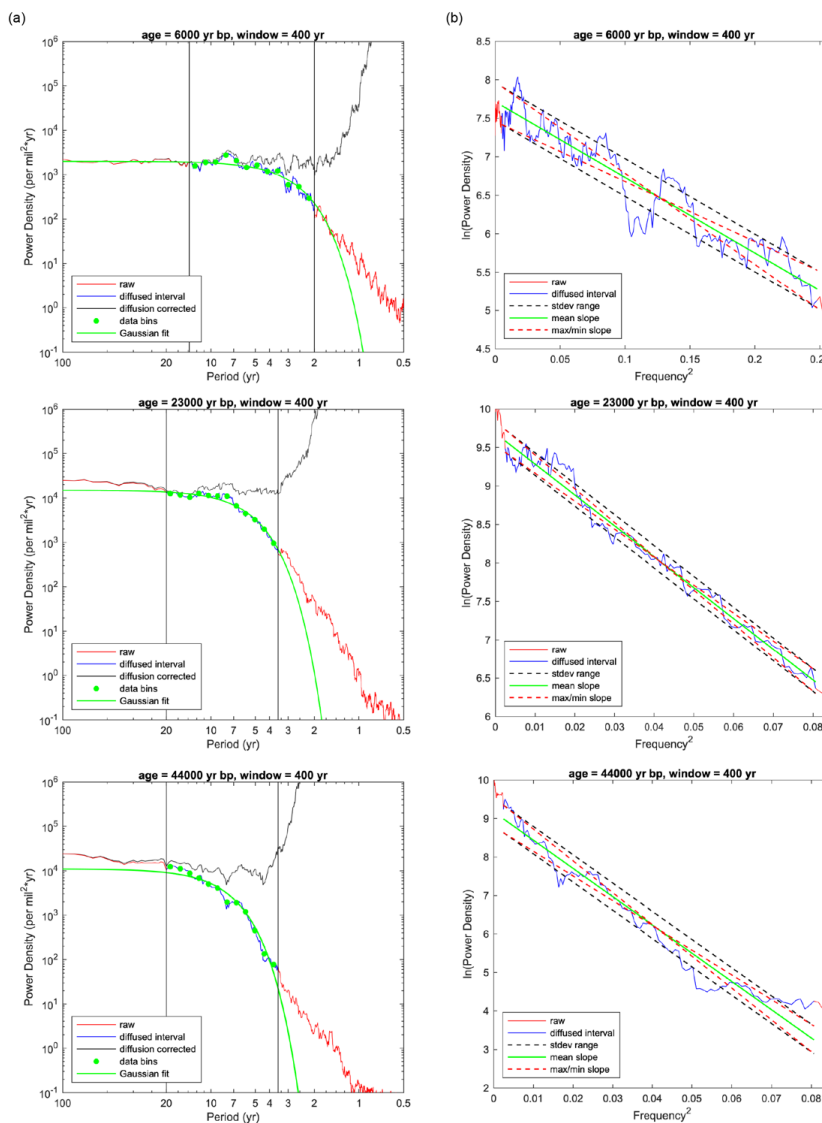
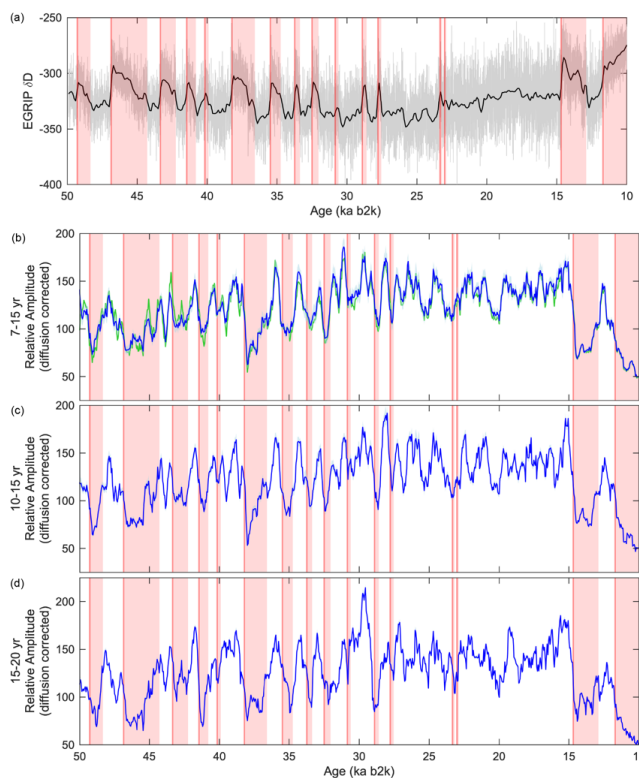


Figure A4 | (a) Examples of 400-year power density spectra (PSD) fitted by Gaussian regression for diffusion correction (progressively older windows towards bottom of panel); Twelve equally spaced logarithmic bins are used in fitting so that higher frequencies with increased data density do not skew correction (b) Examples of uncertainty calculation; maximum and minimum slopes of $[\ln(\text{PSD}) \text{ versus } \text{frequency}^2]$ within one standard deviation represent the high and low uncertainty bounds, respectively

480

485

490



495 **Figure A5** | (a) EGRIP δD (black; window = 400 years; timestep = 50 years) shaded by duration of warm Greenland
Interstadial periods 2-13, the Bølling-Allerød, and Holocene (red; Rasmussen et al., 2014); High-resolution analysis of
(b) 7-15, (c) 10-15 and (d) 15-20 year EGRIP isotopic variability (blue; window = 400 years; timestep = 50 years)
500 using diffusion lengths which have been calculated in the depth domain and converted to the time domain using annual
layer thickness; Results from Fig. 3 (green) are plotted underneath results in panel (b) to demonstrate that the method
of diffusion-length calculation does not affect the lead-lag relationship between variability and the mean

500

505

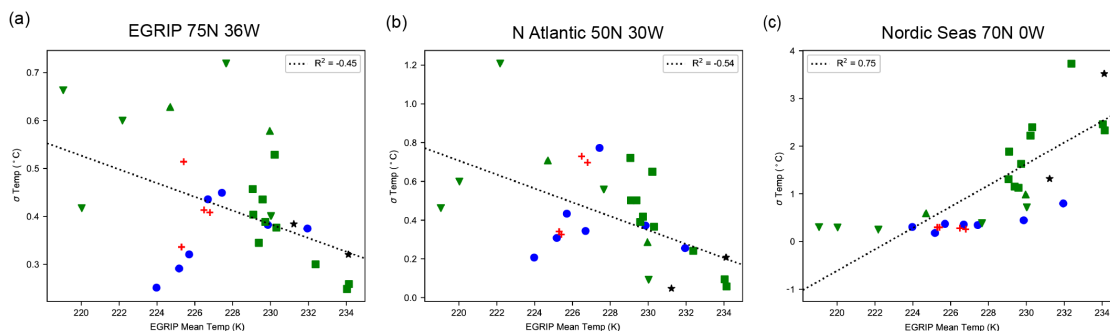


Figure A6 | Individual simulation results for the correlation between 7-15 year temperature variability and EGRIP mean temperature at (a) EGRIP, (b) North Atlantic, and (c) Central Nordic Seas

510

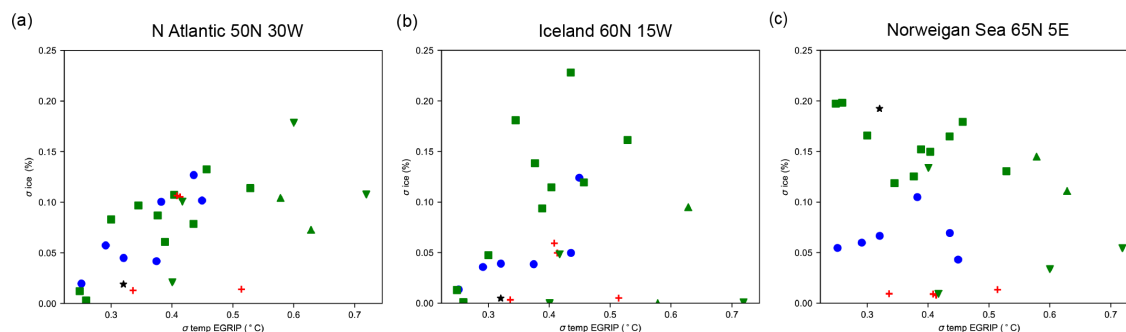


Figure A7 | Individual simulation results for the correlation between 7-15 year sea ice variability and 7-15 year EGRIP temperature variability at (a) North Atlantic, (b) Iceland and (c) Norwegian Sea

515



520 **Date Availability.** EGRIP δD and $\delta^{18}O$ data to 49.9 ka b2k is available through the NSF-Arctic Data Center
(doi:10.18739/A2H41JP05).

Author Contributions. CAB and TRJ contributed to all aspects of this paper. TRJ designed the study. BHV, VM, TRJ
and JWCW developed the continuous flow analysis system. WHGR provided HadCM3 model output. SOR developed
525 the age-depth scale. BMV and BHV co-led the EGRIP water isotope consortium. VM, BHV, RN, TRJ, CAB, KSR,
AGH, WBS, VG, CH, MFK, SEK, PL, FM, JR, MS, GS, and SSJ measured the high-resolution EGRIP water isotope
data. KMC and TRJ developed the spectral techniques for diffusion correction. CAB wrote this article with significant
editorial contributions from TRJ and comments from all authors. TS, CB, BHV, and JWCW were principal
investigators on this project, funded through the National Science Foundation.

530

Competing Interests. At least one of the (co-)authors is a member of the editorial board of *Climate of the Past*.

Acknowledgements. The East Greenland Ice Core Project (EGRIP) was facilitated by collaborations between the
Danish Centre for Ice and Climate, the US Office of Polar Programs (OPP), the National Science Foundation (NSF)
535 and U.S. Air National Guard. The authors acknowledge scientific and logistical support from the entire EGRIP
community.

Financial Support. This research has been supported by the National Science Foundation (grant no. 1804154 and
1804133) and the Niels Bohr Institute at the University of Copenhagen. SOR and GS acknowledges support from the
540 Carlsberg Foundation (ChronoClimate) and the Villum Investigator Project IceFlow (grant no. 16572).



References.

- 545 Armstrong, E., Izumi, K., & Valdes, P. (2022). Identifying the mechanisms of DO-scale oscillations in a GCM: A salt oscillator triggered by the Laurentide ice sheet. *Climate Dynamics*, 60, 1–19. <https://doi.org/10.1007/s00382-022-06564-y>
- Asmerom, Y., Polyak, V. J., & Burns, S. J. (2010). Variable winter moisture in the southwestern United States linked to rapid glacial climate shifts. *Nature Geoscience*, 3(2), Article 2. <https://doi.org/10.1038/ngeo754>
- 550 Blunier, T., & Brook, E. J. (2001). Timing of Millennial-Scale Climate Change in Antarctica and Greenland During the Last Glacial Period. *Science*, 291(5501), 109–112. <https://doi.org/10.1126/science.291.5501.109>
- Blunier, T., Chappellaz, J., Schwander, J., Dällenbach, A., Stauffer, B., Stocker, T. F., Raynaud, D., Jouzel, J., Clausen, H. B., Hammer, C. U., & Johnsen, S. J. (1998). Asynchrony of Antarctic and Greenland climate change during the last glacial period. *Nature*, 394(6695), Article 6695. <https://doi.org/10.1038/29447>
- 555 Boers, N. (2018). Early-warning signals for Dansgaard-Oeschger events in a high-resolution ice core record. *Nature Communications*, 9(1), Article 1. <https://doi.org/10.1038/s41467-018-04881-7>
- Boers, N., Ghil, M., & Rousseau, D.-D. (2018). Ocean circulation, ice shelf, and sea ice interactions explain Dansgaard–Oeschger cycles. *Proceedings of the National Academy of Sciences*, 115(47), E11005–E11014. <https://doi.org/10.1073/pnas.1802573115>
- 560 Brennan, C. E., Meissner, K. J., Eby, M., Hillaire-Marcel, C., & Weaver, A. J. (2013). Impact of sea ice variability on the oxygen isotope content of seawater under glacial and interglacial conditions. *Paleoceanography*, 28(3), 388–400. <https://doi.org/10.1002/palo.20036>
- Broecker, W. S. (1998). Paleocean circulation during the Last Deglaciation: A bipolar seesaw? *Paleoceanography*, 13(2), 119–121. <https://doi.org/10.1029/97PA03707>
- 565 Broecker, W. S., Bond, G., Klas, M., Bonani, G., & Wolfl, W. (1990). A salt oscillator in the glacial Atlantic? 1. The concept. *Paleoceanography*, 5(4), 469–477. <https://doi.org/10.1029/PA005i004p00469>
- Capron, E., Rasmussen, S. O., Popp, T. J., Erhardt, T., Fischer, H., Landais, A., Pedro, J. B., Vettoretti, G., Grinsted, A., Gkinis, V., Vaughn, B., Svensson, A., Vinther, B. M., & White, J. W. C. (2021). The anatomy of past abrupt warmings recorded in Greenland ice. *Nature Communications*, 12(1), Article 1. <https://doi.org/10.1038/s41467-021-22241-w>
- 570 Cruz, F. W., Burns, S. J., Karmann, I., Sharp, W. D., Vuille, M., Cardoso, A. O., Ferrari, J. A., Silva Dias, P. L., & Viana, O. (2005). Insolation-driven changes in atmospheric circulation over the past 116,000 years in subtropical Brazil. *Nature*, 434(7029), Article 7029. <https://doi.org/10.1038/nature03365>
- Dansgaard, W. (1964). Stable isotopes in precipitation. *Tellus*, 16(4), 436–468. <https://doi.org/10.1111/j.2153-3490.1964.tb00181.x>
- 575 Dansgaard, W., Johnsen, S. J., Clausen, H. B., Dahl-Jensen, D., Gundestrup, N. S., Hammer, C. U., Hvidberg, C. S., Steffensen, J. P., Sveinbjörnsdóttir, A. E., Jouzel, J., & Bond, G. (1993). Evidence for general instability of past climate from a 250-kyr ice-core record. *Nature*, 364(6434), 218–220. <https://doi.org/10.1038/364218a0>
- Deplazes, G., Lückge, A., Peterson, L. C., Timmermann, A., Hamann, Y., Hughen, K. A., Röhl, U., Laj, C., Cane, M. A., Sigman, D. M., & Haug, G. H. (2013). Links between tropical rainfall and North Atlantic climate during the last glacial period. *Nature Geoscience*, 6(3), Article 3. <https://doi.org/10.1038/ngeo1712>
- 580 Ditlevsen, P., Ditlevsen, S., & Andersen, K. (2002). The fast climate fluctuations during the stadial and interstadial climate states. *Annals of Glaciology*, 35, 457–462. <https://doi.org/10.3189/172756402781816870>
- Dokken, T. M., Nisancioglu, K. H., Li, C., Battisti, D. S., & Kissel, C. (2013). Dansgaard-Oeschger cycles: Interactions between ocean and sea ice intrinsic to the Nordic seas. *Paleoceanography*, 28(3), 491–502. <https://doi.org/10.1002/palo.20042>
- EPICA Community Members. (2006). One-to-one coupling of glacial climate variability in Greenland and Antarctica. *Nature*, 444(7116), 195–198. <https://doi.org/10.1038/nature05301>
- 590 Gerber, T., Hvidberg, C., Rasmussen, S., Franke, S., Sinnl, G., Grinsted, A., Jansen, D., & Dahl-Jensen, D. (2021). Upstream flow effects revealed in the EastGRIP ice core using a Monte Carlo inversion of a two-dimensional ice-flow model. <https://doi.org/10.5194/tc-2021-63>
- Gkinis, V., Simonsen, S. B., Buchardt, S. L., White, J. W. C., & Vinther, B. M. (2014). NorthGRIP firn temperature reconstruction based on water isotope firn diffusion [dataset]. In *Supplement to: Gkinis, V et al. (2014): Water isotope diffusion rates from the NorthGRIP ice core for the last 16,000 years – Glaciological and paleoclimatic*



- 595 *implications. Earth and Planetary Science Letters*, 405, 132–141, <https://doi.org/10.1016/j.epsl.2014.08.022>.
PANGAEA. <https://doi.org/10.1594/PANGAEA.871566>
- Gordon, C., Cooper, C., Senior, C. A., Banks, H., Gregory, J. M., Johns, T. C., Mitchell, J. F. B., & Wood, R. A. (2000). The simulation of SST, sea ice extents and ocean heat transports in a version of the Hadley Centre coupled model without flux adjustments. *Climate Dynamics*, 16(2–3), 147–168.
600 <https://doi.org/10.1007/s003820050010>
- Greenland Ice-core Project (GRIP) Members. (1993). Climate instability during the last interglacial period recorded in the GRIP ice core. *Nature*, 364(6434), 203–207. <https://doi.org/10.1038/364203a0>
- Hoff, U., Rasmussen, T. L., Stein, R., Ezat, M. M., & Fahl, K. (2016). Sea ice and millennial-scale climate variability in the Nordic seas 90 kyr ago to present. *Nature Communications*, 7(1), 12247.
605 <https://doi.org/10.1038/ncomms12247>
- Huber, C., Leuenberger, M., Spahni, R., Flückiger, J., Schwander, J., Stocker, T. F., Johnsen, S., Landais, A., & Jouzel, J. (2006). Isotope calibrated Greenland temperature record over Marine Isotope Stage 3 and its relation to CH4. *Earth and Planetary Science Letters*, 243(3), 504–519. <https://doi.org/10.1016/j.epsl.2006.01.002>
- Hughes, A. G., Jones, T. R., Vinther, B. M., Gkinis, V., Stevens, C. M., Morris, V., Vaughn, B. H., Holme, C., Markle, B. R., & White, J. W. C. (2020). High-frequency climate variability in the Holocene from a coastal-dome ice core in east-central Greenland. *Climate of the Past*, 16(4), 1369–1386. <https://doi.org/10.5194/cp-16-1369-2020>
- Huybers, P. (2021). pmtmPH.m (<https://www.mathworks.com/matlabcentral/fileexchange/2927-pmtmph-m>), MATLAB Central File Exchange. Retrieved April 13, 2021.
- 615 Johnsen, S., Clausen, H. B., Cuffey, K. M., Schwander, J., & Creyts, T. (2000). Diffusion of stable isotopes in polar firn and ice: The isotope effect in firn diffusion. *Physics of Ice Core Records*, 121–140.
- Jones, T. R., Cuffey, K. M., Roberts, W. H. G., Markle, B. R., Steig, E. J., Stevens, C. M., Valdes, P. J., Fudge, T. J., Sigl, M., Hughes, A. G., Morris, V., Vaughn, B. H., Garland, J., Vinther, B. M., Rozmiarek, K. S., Brashear, C. A., & White, J. W. C. (2023). Seasonal temperatures in West Antarctica during the Holocene. *Nature*, 613(7943), Article 7943. <https://doi.org/10.1038/s41586-022-05411-8>
- 620 Jones, T. R., Cuffey, K. M., White, J. W. C., Steig, E. J., Buizert, C., Markle, B. R., McConnell, J. R., & Sigl, M. (2017). Water isotope diffusion in the WAIS Divide ice core during the Holocene and last glacial. *Journal of Geophysical Research: Earth Surface*, 122(1), 290–309. <https://doi.org/10.1002/2016JF003938>
- Jones, T. R., Roberts, W. H. G., Steig, E. J., Cuffey, K. M., Markle, B. R., & White, J. W. C. (2018). Southern Hemisphere climate variability forced by Northern Hemisphere ice-sheet topography. *Nature*, 554(7692), Article 7692. <https://doi.org/10.1038/nature24669>
- 625 Jones, T. R., White, J. W. C., Steig, E. J., Vaughn, B. H., Morris, V., Gkinis, V., Markle, B. R., & Schoenemann, S. W. (2017). Improved methodologies for continuous-flow analysis of stable water isotopes in ice cores. *Atmospheric Measurement Techniques*, 10(2), 617–632. <https://doi.org/10.5194/amt-10-617-2017>
- 630 Kahle, E. C., Steig, E. J., Jones, T. R., Fudge, T. J., Koutnik, M. R., Morris, V. A., Vaughn, B. H., Schauer, A. J., Stevens, C. M., Conway, H., Waddington, E. D., Buizert, C., Epifanio, J., & White, J. W. C. (2021). Reconstruction of Temperature, Accumulation Rate, and Layer Thinning From an Ice Core at South Pole, Using a Statistical Inverse Method. *Journal of Geophysical Research: Atmospheres*, 126(13), e2020JD033300. <https://doi.org/10.1029/2020JD033300>
- 635 Kindler, P., Guillevic, M., Baumgartner, M., Schwander, J., Landais, A., & Leuenberger, M. (2014). Temperature reconstruction from 10 to 120 kyr b2k from the NGRIP ice core. *Climate of the Past*, 10, 887–902. <https://doi.org/10.5194/cp-10-887-2014>
- Knutti, R., Flückiger, J., Stocker, T. F., & Timmermann, A. (2004). Strong hemispheric coupling of glacial climate through freshwater discharge and ocean circulation. *Nature*, 430(7002), Article 7002.
640 <https://doi.org/10.1038/nature02786>
- Li, C., Battisti, D., & Bitz, C. (2010). Can North Atlantic Sea Ice Anomalies Account for Dansgaard-Oeschger Climate Signals? *Journal of Climate - J CLIMATE*, 23, 5457–5475. <https://doi.org/10.1175/2010JCLI3409.1>
- Li, C., Battisti, D. S., Schrag, D. P., & Tziperman, E. (2005). Abrupt climate shifts in Greenland due to displacements of the sea ice edge: GREENLAND CLIMATE SHIFTS AND SEA ICE. *Geophysical Research Letters*, 32(19), n/a-n/a. <https://doi.org/10.1029/2005GL023492>
- 645 Mojtavavi, S., Wilhelms, F., Cook, E., Davies, S., Sinnl, G., Skov Jensen, M., Dahl-Jensen, D., Svensson, A., Vinther, B., Kipfstuhl, S., Jones, G., Karlsson, N. B., Faria, S. H., Gkinis, V., Kjær, H., Erhardt, T., Berben, S. M. P., Nisancioglu, K. H., Koldtoft, I., & Rasmussen, S. O. (2019). *A first chronology for the East Greenland*



- 650 *Ice-core Project (EGRIP) over the Holocene and last glacial termination* [Preprint]. Proxy Use-Development-Validation/Ice Cores/Holocene. <https://doi.org/10.5194/cp-2019-143>
- North Greenland Ice Core Project Members. (2004). High-resolution record of Northern Hemisphere climate extending into the last interglacial period. *Nature*, 431, 147–151. <https://doi.org/10.1038/nature02805>
- Ortega, P., Swingedouw, D., Masson-Delmotte, V., Risi, C., Vinther, B., Yiou, P., Vautard, R., & Yoshimura, K. (2014). Characterizing atmospheric circulation signals in Greenland ice cores: Insights from a weather regime approach. *Climate Dynamics*, 43(9), 2585–2605. <https://doi.org/10.1007/s00382-014-2074-z>
- 655 Peltier, W. R., & Vettoretti, G. (2014). Dansgaard-Oeschger oscillations predicted in a comprehensive model of glacial climate: A “kicked” salt oscillator in the Atlantic. *Geophysical Research Letters*, 41(20), 7306–7313. <https://doi.org/10.1002/2014GL061413>
- Percival, D., & Walden, A. (1993). *Spectral Analysis for Physical Applications*. Cambridge: Cambridge University Press. doi:10.1017/CBO9780511622762
- 660 Petersen, S. V., Schrag, D. P., & Clark, P. U. (2013). A new mechanism for Dansgaard-Oeschger cycles. *Paleoceanography*, 28(1), 24–30. <https://doi.org/10.1029/2012PA002364>
- Pope, V. D., Gallani, M. L., Rowntree, P. R., & Stratton, R. A. (2000). The impact of new physical parametrizations in the Hadley Centre climate model: HadAM3. *Climate Dynamics*, 16(2-3), 123–146. <https://doi.org/10.1007/s003820050009>
- 665 Rasmussen, S. O., Bigler, M., Blockley, S. P., Blunier, T., Buchardt, S. L., Clausen, H. B., Cvijanovic, I., Dahl-Jensen, D., Johnsen, S. J., Fischer, H., Gkinis, V., Guillevic, M., Hoek, W. Z., Lowe, J. J., Pedro, J. B., Popp, T., Seierstad, I. K., Steffensen, J. P., Svensson, A. M., ... Winstrup, M. (2014). A stratigraphic framework for abrupt climatic changes during the Last Glacial period based on three synchronized Greenland ice-core records: Refining and extending the INTIMATE event stratigraphy. *Quaternary Science Reviews*, 106, 14–28. <https://doi.org/10.1016/j.quascirev.2014.09.007>
- 670 Rehfeld, K., Münch, T., Ho, S. L., & Laepple, T. (2018). Global patterns of declining temperature variability from the Last Glacial Maximum to the Holocene. *Nature*, 554(7692), Article 7692. <https://doi.org/10.1038/nature25454>
- 675 Rimbu, N., & Lohmann, G. (2010). Decadal Variability in a Central Greenland High-Resolution Deuterium Isotope Record and Its Relationship to the Frequency of Daily Atmospheric Circulation Patterns from the North Atlantic Region. *Journal of Climate - J CLIMATE*, 23, 4608–4618. <https://doi.org/10.1175/2010JCLI3556.1>
- Rimbu, N., Ionita, M., & Lohmann, G. (2021). A Synoptic Scale Perspective on Greenland Ice Core $\delta^{18}O$ Variability and Related Teleconnection Patterns. *Atmosphere*, 12(3), Article 3. <https://doi.org/10.3390/atmos12030294>
- 680 Roberts, W. H. G., & Hopcroft, P. O. (2020). Controls on the Tropical Response to Abrupt Climate Changes. *Geophysical Research Letters*, 47(6), e2020GL087518. <https://doi.org/10.1029/2020GL087518>
- Sadatzi, H., Dokken, T., Berben, S., Muschitiello, F., Stein, R., Fahl, K., Menviel, L., Timmermann, A., & Jansen, E. (2019). Sea ice variability in the southern Norwegian Sea during glacial Dansgaard-Oeschger climate cycles. *Science Advances*, 5. <https://doi.org/10.1126/sciadv.aau6174>
- 685 Sadatzi, H., Maffezzoli, N., Dokken, T. M., Simon, M. H., Berben, S. M. P., Fahl, K., Kjær, H. A., Spolaor, A., Stein, R., Vallelonga, P., Vinther, B. M., & Jansen, E. (2020). Rapid reductions and millennial-scale variability in Nordic Seas sea ice cover during abrupt glacial climate changes. *Proceedings of the National Academy of Sciences*, 117(47), 29478–29486. <https://doi.org/10.1073/pnas.2005849117>
- Schulz, M., Paul, A., & Timmermann, A. (2004). Glacial–interglacial contrast in climate variability at centennial-to-millennial timescales: Observations and conceptual model. *Quaternary Science Reviews*, 23(20), 2219–2230. <https://doi.org/10.1016/j.quascirev.2004.08.014>
- 690 Severinghaus, J. P., & Brook, E. J. (1999). Abrupt Climate Change at the End of the Last Glacial Period Inferred from Trapped Air in Polar Ice. *Science*, 286(5441), 930–934. <https://doi.org/10.1126/science.286.5441.930>
- Severinghaus, J. P., Sowers, T., Brook, E. J., Alley, R. B., & Bender, M. L. (1998). Timing of abrupt climate change at the end of the Younger Dryas interval from thermally fractionated gases in polar ice. *Nature*, 391(6663), Article 6663. <https://doi.org/10.1038/34346>
- 695 Simonsen, S. B., Johnsen, S. J., Popp, T. J., Vinther, B. M., Gkinis, V., & Steen-Larsen, H. C. (2011). *Past surface temperatures at the NorthGRIP drill site from the difference in firn diffusion of water isotopes* [Preprint]. Proxy Use-Development-Validation/Ice Cores/Millennial/D-O. <https://doi.org/10.5194/cpd-7-921-2011>
- 700 Steffensen, J. P., Andersen, K. K., Bigler, M., Clausen, H. B., Dahl-Jensen, D., Fischer, H., Goto-Azuma, K., Hansson, M., Johnsen, S. J., Jouzel, J., Masson-Delmotte, V., Popp, T., Rasmussen, S. O., Röthlisberger, R., Ruth, U., Stauffer, B., Siggaard-Andersen, M.-L., Sveinbjörnsdóttir, A. E., Svensson, A., & White, J. W. C.



- (2008). High-Resolution Greenland Ice Core Data Show Abrupt Climate Change Happens in Few Years. *Science*, 321(5889), 680–684. <https://doi.org/10.1126/science.1157707>
- 705 Stocker, T. F., & Johnsen, S. J. (2003). A minimum thermodynamic model for the bipolar seesaw. *Paleoceanography*, 18(4). <https://doi.org/10.1029/2003PA000920>
- Svensson, A., Andersen, K. K., Bigler, M., Clausen, H. B., Dahl-Jensen, D., Davies, S. M., Johnsen, S. J., Muscheler, R., Parrenin, F., Rasmussen, S. O., Rothlisberger, R., Seierstad, I., Steffensen, J. P., & Vinther, B. M. (2008). A 60 000 year Greenland stratigraphic ice core chronology. *Clim. Past*, 11.
- 710 Valdes, P. J., Armstrong, E., Badger, M. P. S., Bradshaw, C. D., Bragg, F., Crucifix, M., Davies-Barnard, T., Day, J., Farnsworth, A., Gordon, C., Hopcroft, P. O., Kennedy, A. T., Lord, N. S., Lunt, D. J., Marzocchi, A., Parry, L. M., Pope, V., Roberts, W. H. G., Stone, E. J., Tourte, G. J. L., & Williams, J. H. T. (2017). The BRIDGE HadCM3 family of climate models: HadCM3Bristol v1.0. *Geoscientific Model Development*, 10(10), 3715–3743. <https://doi.org/10.5194/gmd-10-3715-2017>
- 715 Wagner, J. D. M., Cole, J. E., Beck, J. W., Patchett, P. J., Henderson, G. M., & Barnett, H. R. (2010). Moisture variability in the southwestern United States linked to abrupt glacial climate change. *Nature Geoscience*, 3(2), Article 2. <https://doi.org/10.1038/ngeo707>
- WAIS Divide Project Members. (2015). Precise inter polar phasing of abrupt climate change during the last ice age. *Nature*, 520(7549), Article 7549. <https://doi.org/10.1038/nature14401>
- 720 Whillans, I. M., & Grootes, P. M. (1985). Isotopic diffusion in cold snow and firn. *Journal of Geophysical Research: Atmospheres*, 90(D2), 3910–3918. <https://doi.org/10.1029/JD090iD02p03910>